Environment Canada

National Water Research Institute

Environnement Canada

Institut National de Recherche sur les Eaux
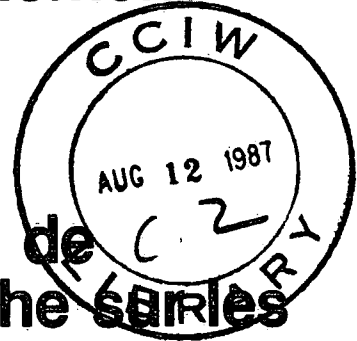
PARTICULATE CONCENTRATIONS IN
LAKE ST. CLAIR AS RECORDED BY A SHIPBORNE
MULTISPECTRAL OPTICAL MONITORING SYSTEM
by
R.P. Bukata, J.H. Jerome and J.E. Bruton

PARTICULATE CONCENTRATIONS IN
LAKE ST. CLAIR AS RECORDED BY A SHIPBORNE
MULTISPECTRAL OPTICAL MONITORING SYSTEM
by
R.P. Bukata, J.H. Jerome and J.E. Bruton

Rivers Research Branch
National Water Research Institute
Canada Centre for Inland Waters
Burlington, Ontario, Canada
NWRI Contribution #87-43

MANAGEMENT PERSPECTIVE

The use of ship surveys defined by a pre-determined optimal set of discrete sampling stations has long been recognized as being an indisputably essential component of programs seriously dedicated to the monitoring and assessment of the bio-chemical/physical properties of large lake and river systems. While the contributions of discrete point sampling programs are of inarguable value, such point sampling activities are forced to contend with at least one severe limitation, namely the loss of comparable information for aquatic regimes between the discrete sample stations. These discontinuities in the time-space continuum could result in serious uncertainties being reflected within the deductions based on discrete sampling information, particularly when such discrete sampling activities are performed on aquatic resources subjected to short-term fluctuations and/or large scale variations in any or all of the physical, chemical, and biological parameters comprising their makeup.

This communication describes a ship-mounted optical device which is intended to supplement, in certain situations, the discrete sampling ship surveys, by providing the capability to continuously monitor, in a remote manner, the aquatic resource while the research vessel is in transit between the fixed monitoring stations. The ship-mounted remote sensing device is a Multispectral Optical Monitoring System (MOMS) comprised of an upward-viewing four-channel radiometer subsystem with rotating solar occluder (which continually

monitors the downwelling solar and sky irradiance) and a downward-viewing four-channel radiometer subsystem (which continually monitors the upwelling radiance from the water). An optical model is developed which allows the conversion of the downwelling irradiances and upwelling radiances into spectral values of the subsurface irradiance reflectance (volume reflectance) normalized to a standard solar zenith angle and a standard downwelling light field. This normalized multispectral subsurface volume reflectance is then utilized to evaluate the capability of effectively conducting, from a moving research vessel, a continuous monitor of the total seston and suspended sediment concentrations in the generally turbid, shallow waters of Lake St. Clair. Examples of ship/MOMS transects of Lake St. Clair are presented which display very good agreement between the laboratory-analyzed concentrations of seston and suspended sediments from collected samples, and between-station concentrations remotely estimated by the continuous optical data collected and interpreted by MOMS.

ABSTRACT

Methodology is developed to convert the upwelling multispectral radiance observed by a ship-mounted dual radiometer reflectance system into the subsurface volume reflectance normalized to a standard solar zenith angle and a standard downwelling light field. This normalized multispectral subsurface volume reflectance is then utilized to evaluate the capacity of effectively conducting, from a moving research vessel, a continuous monitor of the total seston and suspended sediment concentrations in the generally turbid, shallow waters of Lake St. Clair. Good agreement is obtained between remotely predicted and directly sampled concentrations of both seston and suspended sediments.

PERSPECTIVE-GESTION

Il est reconnu depuis longtemps que les relevés en navire portant sur un ensemble optimal de points d'échantillonnage discontinu et prédéterminé sont essentiels dans la surveillance et l'évaluation des propriétés biochimiques et physiques des eaux des grands lacs et des grands cours d'eau lorsqu'on veut faire un travail sérieux. L'utilité de ces relevés est incontestable, mais l'échantillonnage discontinu présente au moins un grand inconvénient : on n'obtient aucune donnée comparable sur les régimes aquatiques entre chaque point de relevé. Ces intervalles dans l'espace et le temps peuvent être à l'origine d'incertitudes importantes, incertitudes qui influeront sur les déductions qu'on pourra faire à l'analyse des renseignements recueillis, surtout si l'on étudie un milieu aquatique dont certaines des caractéristiques physiques, chimiques et biologiques, sinon toutes, fluctuent rapidement ou varient beaucoup.

On décrit ici un appareil optique qui se monte sur le navire de recherche et qui devrait permettre de compléter, dans certaines conditions, les résultats des relevés ponctuels en donnant la possibilité de surveiller continuellement le milieu aquatique par télédétection, alors que le navire de recherche se déplace entre deux points de contrôle. Il s'agit de l'appareil de surveillance optique multispectral (ASOM) : il se compose d'un radiomètre à quatre canaux avec obturateur solaire, orienté vers le haut (qui permet de contrôler le rayonnement solaire et la lumière du ciel) et d'un radiomètre à

quatre canaux, orienté vers le bas (qui permet de contrôler les rayonnements ascendants dans l'eau). On est à mettre au point un modèle optique pour convertir l'énergie des rayonnements descendants et ascendants en valeurs de luminance spectrale dans la couche sous-jacente (luminance de volume) normalisées en fonction d'un angle de zénith et d'un champ lumineux standard. La luminance de volume sous-jacente multispectrale normalisée sert à déterminer avec quelle efficacité on peut contrôler en continu, depuis le navire de recherche en mouvement, les concentrations totales de seston et de matières solides en suspension dans les eaux peu profondes, généralement troubles, du lac Sainte-Claire. On donne des exemples de transects contrôlés au moyen de l'ASOM dans le lac Sainte-Claire pour montrer que les concentrations de seston et de matières solides en suspension mesurées en laboratoire dans les échantillons recueillis concordent très bien avec les valeurs déterminées par contrôle optique continu en télédétection au moyen de l'ASOM.

RÉSUMÉ

On est à mettre au point la méthodologie de la conversion de l'énergie des rayonnements ascendants, observés au moyen d'un appareil de radiométrie double monté sur un navire, en valeurs de luminance de volume sous-jacente normalisées en fonction d'un angle de zénith et d'un champ lumineux descendant standard. Ces valeurs servent à déterminer avec quelle efficacité on peut contrôler en continu, depuis un navire de recherche en mouvement, les

concentrations totales de seston et de matières solides en suspension dans les eaux peu profondes et généralement troubles du lac Sainte-Claire. Les concentrations de seston et de matières solides en suspension mesurées en laboratoire concordent bien avec les valeurs déterminées par télédétection.

1. INTRODUCTION

The difficulties in applying remote sensing techniques to the estimation of water quality parameters in natural water masses as optically complex as those found in inland lake systems have long been known to a multitude of workers on a global scale. Recently we have detailed an attempt (Bukata et al., 1985) to evaluate both the relative virtues and distinct limitations that are associated with the utilization of direct measurements of lake optical parameters [such as the subsurface irradiance reflectance spectrum (volume reflectance spectrum), $R_v(\lambda)$] to infer water quality indicators (such as the concentrations of chlorophyll a, suspended minerals, and dissolved organic carbon). This work, performed in the dynamically and optically complex waters of Lake Ontario, resulted from coordinated efforts of optical and water quality data collection, multiple regression, radiative transfer theory, and optimization technique analysis which interwove in a manner designed to a) obtain the scattering and absorption cross sections (i.e. the amount of scattering and absorption per unit concentration) for chlorophyll a, suspended mineral, and dissolved organic carbon over the range of visible wavelengths, b) use these optical cross-section spectra to simulate the subsurface irradiance reflectance spectrum that would be anticipated for any combination of chlorophyll, suspended mineral, and dissolved organics, and c) compare, through optimization methodology, these simulated subsurface irradiance spectra with in situ

measurements of the volume reflectance as a means of estimating the water quality concentrations contributing to the observed subsurface optical spectrum.

The work described in Bukata et al. (1985) restricted itself to volume reflectance spectra measured just beneath the air-water interface. Clearly, before such water quality modelling may be applied to remote sensing devices such as aircraft or earth-orbiting satellites, the subsurface irradiance spectrum must be transferred through the air-water interface, converted to an upwelling radiance spectrum, corrected for surface reflection, and transferred through an atmospheric mass to a downward-viewing remote sensing device.

This paper deals with such a transition from a vantage point within the water mass to a vantage point on a remote platform above the water mass. However, it stops considerably short of dealing with a high altitude satellite or aircraft. The remotely-sensed platform considered herein is ship-mounted, a situation for which it is not unreasonable to assume that the effects of atmospheric attenuation and scattering may be considered negligible. The remainder of this communication will present a brief description of this Multispectral Optical Monitoring System (MOMS) which is comprised of a dual radiometer reflectance system, ship-mounted so that one radiometer views the upper hemisphere while the other has a viewing direction vertically downwards, discuss its analyses/interpretation methodology, and present some initial results of its use in Lake St. Clair which forms part of the Canada/United States border in the Great Lakes

System. Being a ship-mounted spectral radiometer system, MOMS, in essence, represents an extremely slow moving, low-altitude, orbiting environmntal satellite which affords the opportunity for a quasi-continuous water quality monitoring activity.

2. MULTISPECTRAL OPTICAL MONITORING SYSTEM (MOMS)

Figure 1 illustrates a schematic representation of the boom-mounted remote sensing device used in this study of Lake St. Clair. Each of the radiometer subsystems consists of a commercial Exotech four-channel radiometer. The spectral bands covered correspond to those of the LANDSAT/THEMATIC MAPPER blue, green, and red bands and the LANDSAT/MULTI SPECTRAL SCANNER infra red band in the wavelength intervals (0.45 μ - 0.52 μ), (0.52 μ - 0.60 μ), (0.63 μ - 0.69 μ) and (0.8 μ - 1.1 μ), respectively. The upward-viewing subsystem, designed to obtain data on the variability of incident radiation conditions, is equipped with an enclosing hemispherical plexiglass window and a rotating solar occluder assembly. The field of view of the upward-viewing radiometer assembly is 2π sterads, cosinusoidal, and the solar occluder rotation period of 45 seconds allows for the continual monitoring of total (direct and diffuse) and diffuse incident spectral irradiance. The field of view of the downward-viewing radiometer assembly is 15° corrected for ship's roll and pitch, and thus allows for continuous monitoring of the near surface upwelling spectral radiance from the lake water.

Detailed descriptions of the electro-optical, mechanical, and physical characteristics of MOMS, along with installation and mounting details, operating procedures and performance specifications and indicators, functional block and wiring diagrams, and data acquisition and storage techniques may be found in the report by Watson et al. (1982).

3. ANALYSES METHODOLOGY

If H_{sun} and H_{sky} represent the spectrally-dependent downwelling irradiances from the sun and sky, respectively, and H_{LOW} and H_{HIGH} represent the spectrally-dependent downwelling irradiances recorded by the upward-viewing radiometer assembly with the solar occluder blocking and not blocking the solar disk from the sensor's field of view, respectively, then it is evident that

$$H_{sun} = (H_{HIGH} - H_{LOW})/T_{COVER} \qquad (1)$$

and

$$H_{sky} = H_{LOW}/mT_{COVER} \qquad (2)$$

where

T_{COVER} = transmission of the hemispherical plexiglass cover plate

m = fraction of sky not occluded

The upwelling radiance L_{Up} from the surface is given by

$$L_{Up} = H_{UpW} T_{SURF}/Q + f_1 H_{sky} f_2 H_{sun} \qquad (3)$$

where H_{UpW} =   upwelling irradiance below the water surface

Q =   ratio of upwelling irradiance below the water surface to the upwelling nadir radiance below the water surface

T_{SURF} =   transmission of nadir radiance through the air-water interface including correction for the n^2 radiance law (n being the relative refractive index of the water)

f_1 =   ratio of the upwelling radiance entering the FOV of the sensor (originating from surface-reflected diffuse skylight) to the downwelling sky irradiance

f_2 =   ratio of the upwelling radiance entering the FOV of the sensor (originating from surface-reflected direct sunlight) to the downwelling solar irradiance.

From equation (3), the upwelling irradiance below the water surface is given by

$$H_{UpW} = Q [L_{Up} - f_1 H_{sky} - f_2 H_{sun}] / T_{SURF} \qquad (4)$$

The downwelling irradiance H_{DnW}, below the water surface is given by

$$H_{DnW} = f_3 H_{sky} + f_4 H_{sun} \qquad (5)$$

where f_3 = fraction of downwelling sky irradiance transmitted into the water

f_4 = fraction of downwelling solar irradiance transmitted into the water

The spectrally-dependent diffuse irradiance reflectance or volume reflectance R_V, just beneath the surface of the water, is then obtained as the ratio of equation (4) to equation (5), i.e.

$$R_V = \frac{H_{UpW}}{H_{DnW}}$$

$$= \frac{Q[L_{Up} - f_1 H_{sky} - f_2 H_{sun}]}{T_{SURF}[f_3 H_{sky} + f_4 H_{sun}]} \qquad (6)$$

In order to facilitate the conversion of the above surface optical parameters L_{Up} (upwelling spectral radiance), H_{sky} (downwelling sky irradiance), and H_{sun} (downwelling solar irradiance) directly measured by MOMS, into the subsurface optical parameter R_V (volume reflectance), not directly measured but required to infer the scattering and absorption processes occurring

within the water column, it is convenient to express the fractions f_1, f_2 f_3, and f_4 in the following terms:

$$f_1 = \alpha \rho_0 + \beta_1 \qquad (7)$$

where α =   the spectrally-dependent ratio of downwelling zenith sky radiance to downwelling sky irradiance

         ρ_0 =   Fresnel reflectivity for vertical incidence (i.e. zenith angle of 0°)

         β_1 =   ratio of the upwelling radiance entering the FOV of the sensor (a consequence of sky irradiance being reflected by surficial waves) to the downwelling sky irradiance.

From Gordon (1969), the value of β_1 for wind speeds of 0-10 m sec^{-1} is taken to be zero. Since this condition is satisfied throughout this investigation, equation (7) may be simplified to

$$f_1 = \alpha \rho_0 \qquad (8)$$

The Fresnel reflectivity ρ_0 at $\theta = 0°$ is 0.0212 for a relative index of refraction n=1.341. Equation (8) then becomes

$$f_1 = 0.0212 \alpha \qquad (9)$$

An expression for f_2 (reflection of solar irradiance due to surficial waves) may be obtained for waters displaying small to moderate suspended sediment concentrations by assuming that the volume reflectance response in the near infra-red wavelengths may be confidently taken to be zero. For this condition, the infra-red radiance response L_{Up} may be written

$$L_{Up} = f_1 H_{sky} + f_2 H_{sun}$$

from which

$$f_2 = \frac{L_{Up} - H_{sky} \rho_0 \alpha}{H_{sun}} \tag{10}$$

where L_{Up}, H_{sky}, H_{sun}, and α are the appropriate values of these parameters for the infra-red channel.

For the case of highly sediment-laden waters such as typically comprise Lake St. Clair, however, the assumption of zero volume reflectance observable just above the air-water interface for near-infra-red wavelengths is not valid. Consequently, equation (10) is not applicable to Lake St. Clair.

As described in Maul (1985), the radiance reflected from the water surface due to wave action ($f_2 H_{sun}$) may be expressed as

$$f_2 \; H_{sun} \; = \; \frac{\rho(\omega) \; H_{sun} \; \exp\left[-\dfrac{\tan^2\delta}{S^2}\right]}{4\pi S^2 \; \cos\psi \; \cos^4\delta}$$

from which

$$f_2 \; = \; \frac{\rho(\omega) \; \exp\left[-\dfrac{\tan^2\delta}{S^2}\right]}{4\pi S^2 \; \cos\psi \; \cos^4\delta} \tag{11}$$

where ω = solar angle of incidence causing reflection into the FOV of the sensor

$\rho(\omega)$= Fresnel reflectivity for incident angle ω

ψ = zenith angle of the sensor (0° for the configuration considered herein)

δ = wave slope required to produce observable solar glitter at the sensor

S^2 = mean square wave slope

Ambient conditions under which MOMS was utilized in Lake St. Clair included a) a range of solar zenith angles 40° to 65° (resulting in ω values ranging from 20° to 32.5°) and b) maximum wind speeds of 5 m sec^{-1}. These conditions resulted in negligible values of f_2 ranging from 8.3×10^{-8} to 7.1×10^{-4}. Therefore, for this study f_2 was confidently taken to be zero, suggesting that surface glitter from the sun was not even a minor contributor to the measured above water radiance.

$$f_3 \; = \; 1 - (\rho_{sky} + \beta_3) \tag{12}$$

where ρ_{sky} =   Fresnel reflectivity of the sky irradiance

β_3 =   fraction of sky irradiance which is reflected due to surficial waves (β_3 is a negative fraction in this instance since the wave action serves to inhibit reflection from its surface)

From Jerlov (1984), ρ_{sky} may be considered to have the value 0.066. Values of β_3 are related to wind speed and possess values of -0.010 for a wind speed of 4 m sec^{-1} (Payne, 1972) and -0.014 for a wind speed of 7 m sec^{-1} (Cox and Munk, 1955). For the current work a value of β_3 = -0.010 was used. From equation (12), this yields a value of f_3 = 0.944.

$$f_4 = 1 - (\rho(\theta) + \beta_4) \tag{13}$$

where $\rho(\theta)$ =   Fresnel reflectivity of solar irradiance for solar zenith angle θ

β_4 =   fraction of solar irradiance which is reflected due to surficial waves

From Cox and Munk (1955), the term $[\rho(\theta) + \beta_4]$ may be mathematically expressed as the series

$$\rho_w(\theta) = \rho(\theta) + \beta_4 = \rho(\theta) \left\{ \frac{1}{2} \left[1 + I(k) \right] + \frac{1}{2} \pi^{-\frac{1}{2}} aSe^{-k^2} \right.$$

$$+ \frac{1}{4} bS^2 \left[1 + I(k) - 2\pi^{-\frac{1}{2}} ke^{-k^2} \right]$$

$$\left. + \frac{1}{4} cS^2 \left[1 + I(k) + \ldots \ldots \ldots \right] \right\} \tag{14}$$

where S^2 =   mean square wave slope

= $0.003 + (0.512 \times 10^{-2} \times \text{wind speed})$

k = $(2S)^{-1} \cot \theta$

$$I(k) = 2\pi^{-\frac{1}{2}} \int_o^k e^{-t^2} dt$$

$F = \rho(\theta) \cos \theta$

$$a = \frac{1}{F} \frac{dF}{d\theta}$$

$$b = \frac{1}{2} + \frac{1}{2F} \frac{d^2F}{d\theta^2}$$

$$c = \frac{1}{2} + \frac{\cot\theta}{2F} \frac{dF}{d\theta}$$

Therefore, $f_4 = 1 - \rho_w(\theta)$ \hfill (15)

Collecting equations (7), (11), (12), and (15) and substituting into equation (6) yields the general expression for the spectrally-dependent volume reflectance R_v observable just below the water surface

$$R_V = \frac{Q\left\{L_{Up} - (\bar{\alpha}\rho_0 + \beta_1) H_{sky} - \dfrac{\rho(\omega)\exp\left[-\dfrac{\tan^2\delta}{S^2}\right] H_{sun}}{4\pi S^2 \cos\psi \cos^4\delta}\right\}}{T_{SURF}\left\{[1 - (\rho_{sky} + \beta_3)] H_{sky} + [1 - \rho_w(\theta)] H_{sun}\right\}} \qquad (16)$$

Simplifying the general equation (16) into a particular equation applicable to the b_1, f_2, β_3 and β_4 values pertinent to the current investigation yields

$$R_V = \frac{Q\left\{L_{Up} - 0.0212\,\alpha\,H_{sky}\right\}}{T_{SURF}\left\{0.944\,H_{sky} + [1 - \rho_w(\theta)]\,H_{sun}\right\}} \qquad (17)$$

From the MOMS sensor configurations and physical properties, the transmission of the hemispherical plexiglass cover, T_{COVER} was measured to be 0.923 and the fraction of the sky m not occluded by the rotating occluder was 0.9497. A value of $T_{SURF} = 0.544$ for a relative index of refraction of 1.341 was chosen (Duntley et al. 1974). The governing equation for the data collected remotely by MOMS over Lake St. Clair thus becomes:

$$R_V = \frac{Q\,(L_{Up} - 0.0242\,\alpha\,H_{LOW})}{0.5859\,H_{LOW} + 0.5894\,[1 - \rho_w(\theta)]\,(H_{HIGH} - H_{LOW})} \qquad (18)$$

where L_{Up} is the spectrally-dependent values of upwelling radiance recorded continuously by the downward-viewing four-channel radiometer assembly, H_{HIGH} and H_{LOW} are the spectrally-dependent values of downwelling irradiance recorded continuously by the periodically

solar-occluded upward-viewing four-channel radiometer assembly, Q is the ratio of upwelling irradiance below the water surface to the upwelling nadir radiance below the water surface, α is the spectrally-dependent ratio of downwelling zenith sky radiance to downwelling sky irradiance, and $\rho_w(\theta)$ is the solar irradiance reflectance term given by equation (14). Each of Q, α, and $\rho_w(\theta)$ must be calculated for each of the R_V values to be determined.

Values of α were obtained through empirical relationships between sky irradiance and zenith sky radiance obtained prior to the on-board use of MOMS. Both of the four-channel radiometer assemblies were positioned in an upward-viewing configuration. In such a configuration the normally upward-viewing irradiance system continued to monitor the downwelling irradiances, while the normally downward-viewing radiance system enabled a simultaneous monitoring of the zenith sky radiance.

Monte Carlo simulations of radiative transfer processes were used to estimate appropriate values of Q. Absorption and scattering coefficients and backscattering probabilities were varied over ranges considered to be typically representative of Great Lakes water masses (Bukata et al., 1979) and the salient results of this Monte Carlo simulation are depicted in Figure 2. Herein are plotted the estimated values of Q (upwelling irradiance below the water surface divided by that upwelling radiance just below the water surface that would refract into a 15° sensor FOV just above the water surface assuming 100% transmission through the air-water interface) against solar

zenith angle θ. Curve A represents a relatively large backscattering probability (0.044) while Curve B represents a relatively low backscattering probability (0.013). The ratio of scattering to absorption was observed to possess a minimal impact on the curves of Figure 2. For the purpose of this work, Curve C which represents the arithmetic means of Curves A and B was used in the determination of Q. For the range of solar zenith angles appropriate to the Lake St. Clair measurements (40° to 65°), values of Q varied from 3.92 to 4.66 (these may be compared to the fixed value of 5.08 reported by Duntley et al. (1974), although conceivably for a detector of FOV other than 15°).

One further mathematical correction must be made to the determined value of R_V. Since the continuous MOMS data stream is collected under temporally-varying conditions of solar zenith angle θ and relative fractions of diffuse and direct downwelling radiation, it is necessry to normalize the subsurface volume reflectance R_V to a standard solar zenith angle and a standard downwelling radiation. If the fraction of total radiation which is diffuse is denoted by F, and the fraction of total radiation which is direct is denoted by (1-F), then

$$R_V(\theta,F) = (1 - F) R_{VS}(\theta) + FR_{VD} \tag{19}$$

where $R_{VS}(\theta)$ = the volume reflectance for direct downwelling radiation (R_{VS} is dependent on θ)

       R_{VD} = the volume reflectance for diffuse downwelling radiation (R_{VD} is independent of θ)

Another Monte Carlo simulation was established to determine the impact on $R_{VS}(\theta)$ of varying θ. Results from the Monte Carlo simulation are illustrated in Figure 3 wherein is plotted the ratio $R_{VS}(\theta)/R_{VS}(0)$ (i.e. the ratio of the subsurface volume reflectance for a solar zenith angle θ to the subsurface volume reflectance for a solar zenith angle of $0°$) as a function of the inverse of the cosine of the refracted angle θ_r. The straight line relationship is defined by

$$R_{VS}(\theta) = \frac{R_{VS}(0)}{\cos \theta_r} \qquad (20)$$

where $\theta_r = \sin^{-1}(\frac{\sin\theta}{n})$

The value of R_{VD} from the Monte Carlo simulation was determined to be

$$R_{VD} = 1.165 \; R_{VS}(0) \qquad (21)$$

Substituting equations (20) and (21) into equation (19) and rearranging terms yields

$$R_{VS}(0) = \frac{R_V(\theta,F)}{(1.165F + \frac{(1-F)}{\cos \theta_r})} \qquad (22)$$

It is this normalized value $R_{VS}(0)$ of the subsurface volume reflectance which is utilized in the current above surface investigation of the water masses comprising Lake St. Clair.

3. DATA SAMPLING LOGISTICS

Figure 4 illustrates a schematic map of Lake St. Clair upon which is superimposed a set of fixed water sampling stations at which water was collected and laboratory analyzed for total seston and suspended sediment concentrations. Transmission measurements were also performed at these stations utilizing a 0.25 m path length Martek XMS transmissometer equipped with a Wratten 45 filter (0.485 μ). MOMS, mounted on a 4.5 m articulated boom, was extended from the bow of the research vessel CSS ADVENT in a manner such as to maintain a 4.5 m height above the water surface for the downward-viewing radiometer assembly. Four visitations to Lake St. Clair were made during September 1985.

The 15° FOV of the radiance radiometer allows a monitoring of optical return from a circular surficial area of diameter 1.2 m. Extending MOMS a distance of 4.5 m in advance of the ship effectively eliminates the influence of bow waves and ship shadow contamination of the sensor FOV (with the exception of solar zenith angles > 45° for the sun located directly aft).

In order to allow on-board adjustment to changing conditions of encountered water masses, MOMS is equipped with automatic gain selectors which provide each sensor with the capacity to maintain signal outputs in the mid-range of each gain setting. The voltage outputs from the assembly of eight sensors (four upward-viewing and

four downward-viewing) are recorded by a Sea Data logger at a rate of 2 hertz. This recording rate enabled a measurement of L_{Up} and H_{HIGH} every 0.5 seconds and a measurement of H_{LOW} every 45 seconds.

Such continual monitoring performed from a moving vehicle results in a greatly increased volume of data sets on which analysis may be performed. This, in turn, provides the capability of obtaining considerably more spatial information than can be obtained from surveillance techniques restricted to point sampling. For an average ship speed of 10 knots, the 2 Hz sampling rate provides a data set every 2.6 metres along the ship track. A 135 m cassette data tape will record L_{Up}, H_{HIGH} and H_{LOW} for about 11 hours or 200 km of ship track.

4. RELATIONSHIPS AMONG SPECTRAL VOLUME REFLECTANCE, SESTON, AND SUSPENDED SEDIMENT

Regressions were performed between three of the spectral upwelling radiance channels (green, red, and near infra-red) and the laboratory analyzed seston and suspended sediment concentration values obtained at the sampling stations.

Elsewhere (Bukata et al., 1985) are presented detailed discussions on the complexities encountered when attempting to utilize monochromatic subsurface irradiance reflectance (volume reflectance) measurements to infer water quality parameters from natural waters

displaying a range of concentration values for a variety of distinct scattering and absorption centres. In particular, the oftentimes total inability to extract the optical impact of chlorophyll a concentrations from the overwhelming optical influences generated by variability in the concurrent presence of suspended solids and dissolved organic substances is well illustrated. However, for water masses such as found in the shallow waters of Lake St. Clair in which the normally encountered suspended sediment concentrations are the predominant source of subsurface optical interactions, single band monochromatic volume reflectance measurements may be of considerable significance.

As discussed and displayed elsewhere (see Figures 28 through 32, Bukata et al., 1985), the theoretically anticipated relationships involving the spectral volume reflectance and suspended mineral concentrations in natural waters are decidedly non-linear over substantial ranges of suspended mineral concentration. Distinct asymptotic behaviour is observed at both very small and relatively large concentrations of suspended load. For the range of suspended load encountered in this Lake St. Clair study (2.5 - 20 g m^{-3}), these non-linear asymptotic relationships were approximated by an exponential curve of the form

$$\text{concentration} = A\, e^{kR_{VS}(0)} \tag{23}$$

where A and k are both constants.

Figures 5 and 6 illustrate the exponential fit of the regressions between the green volume reflectance (0.52 μ - 0.60 μ) and the concentrations of the total seston and suspended sediments, respectively. The data points utilized in these figures represent one point per water sampling station, with the volume reflectance value being determined as the average volume reflectance appropriate to the continuous recording of the upwelling radiance while the research vessel was on station. Figures 7 and 8 illustrate the corresponding exponential regressions for the red volume reflectance (0.63 μ - 0.69 μ) while Figures 9 and 10 illustrate the corresponding exponential regressions for the volume reflectance in the near infra-red wavelengths (0.8 μ - 1.1 μ).

The exponential regressions obtained from Figures 5 through 10 are given in Table I wherein the concentration of seston is indicated by S (g m^{-3}) and the concentration of suspended sediments is indicated by SS(g m^{-3}). The correlation coefficients r and the standard deviation of the errors σ are also listed.

Clearly, the relationships involving the visible wavelength volume reflectances and the seston and sediment concentrations display comparable reliability, a reliability which is substantially greater than those of the corresponding relationships involving the near infra-red volume reflectance.

The remainder of this communication will restrict its consideration to the exponential relationships involving the visible green R_{VG} and visible red R_{VR} volume reflectances. While these exponential relationships are considered operational equations for

this Lake St. Clair study, it must be noted that extrapolation of such exponential empirical relationships to include volume reflectance values substantially below or above the range of values encountered in the regression analysis is fraught with uncertainty. For example, Table I suggests that values of seston concentrations below 1.43 g m^{-3} and 2.22 g m^{-3} and values of suspended sediment concentrations below 1.06 g m^{-3} and 1.69 g m^{-3} cannot be detected by R_{VG} and R_{VR}, respectively. Obviously, should very small or very large volume reflectance values be observed there are mathematical extrapolation techniques which may be applied to modify the mid-range exponential curves arising from the regression exercise. However, since the range of volume reflectances observed in this investigation were well within the range of values depicted in Figures 5 to 10, no such extrapolation techniques were deemed necessary in this work.

5. SESTON AND SUSPENDED SEDIMENT CONCENTRATIONS IN LAKE ST. CLAIR

From the continuously recorded values of L_{Up}, H_{HIGH}, and H_{LOW}, equation (18) was used to calculate the corresponding spectral values of the subsurface volume reflectance R_V. Equation (22) was then used to normalize these R_V values to a fixed solar zenith angle of 0°, viz, $R_{VS}(0)$. These $R_{VS}(0)$ spectral values were then used in conjunction with the equations listed in Table I to provide remote estimates of the seston and suspended sediment concentrations along the ship track in Lake St. Clair.

Figure 11 illustrates the results of the ship transect of September 13, 1985. Herein are plotted the calculated seston concentrations in g m^{-3} (based on 30 sec averages of the continuously determinable values of $R_{VS}(0)$ in the visible red MOMS channel (0.63 μ - 0.69 μ) as a function of both time and ship location. The continuous curve represents the predicted values of seston concentrations based on the continuous operation of MOMS. The non-continuous horizontal bars represent the values of seston concentrations determined from the water samples collected at the fixed monitoring stations, the length of the horizontal bar representing the time spent at the station. One very apparent discrepancy between these two sets of seston values, particularly for the first five station visitations, is the consistently higher values of seston recorded by the in situ water sampling techniques as compared to the values remotely determined by MOMS. One very probable cause for this is bottom sediment resuspension generated by the ship's backwash. The occurrence of such sediment-resuspension is further suggested by the very noticeable increased "spiking" in the seston concentrations determined remotely by MOMS at the station locations. A possible explanation for MOMS consistently recording values of seston concentrations lower than those recorded via direct water collection may be found in the fact that MOMS is boom-mounted in advance of the ship while the direct sampling occurs off mid-ship. Clearly, therefore, while both MOMS and direct sampling techniques are considering water masses which are representative of the aquatic

region under study, the particular water masses to which each is directly exposed are not identical, particularly when shallow waters are significantly agitated by the measurement process. It is further seen from Figure 11 that as the ship transect progressed from the very shallow (2-3 metres) near-shore stations to the deeper (5-6 metres) off-shore stations, the discrepancies between MOMS and direct sampling decreased in magnitude.

While Figure 11 represents a transect from the eastern shore of Lake St. Clair to roughly mid lake, Figure 12 represents a cross-lake transect from west to east taken on September 14, 1985, again using the upwelling red radiance (0.63 μ - 0.69 μ) continuously recorded by MOMS. In this instance considerably less discrepancies are apparent between the on-station direct sampling and the on-station remote sampling, suggesting that the problem of bottom-resuspension was under considerably more control than it was the day before. However, here too, it is seen that the "spiking" is more prominent in the shallower near shore aquatic regimes than in the offshore waters.

It is also clearly seen, however, that both the east and west nearshore regions are characterized by significantly higher concentrations of total suspended material than the slightly deeper mid-lake regions. Also very noticeable in the cross-lake transect is the increased seston concentrations between sampling stations 66 to 69. This corresponds to the location and immediate environs of the artificially deepened shipping channel through Lake St. Clair. The increased suspended material both predicted by MOMS and measured by direct sampling are undoubtedly a consequence of bottom resuspension

initiated by ship traffic. A careful perusal of Figures 11 and 12, reveal that the major discontinuities in the MOMS curves occur when the vessel is both arriving at and departing from the sampling station. Clearly, if future work of this type is to be considered, more serious thought must be assigned to field logistics and in situ data gathering procedures, to ensure that the measurement processes do not adversely impact the scientific purpose of the mission.

Figures 13 and 14 are the green band (0.52 μ - 0.60 μ) equivalents of the red band Figures 11 and 12. Once again the remotely determined MOMS estimates of seston concentrations are displayed as the continuous curve while the discontinuous horizontal bars represent the seston concentrations measured by direct sampling at the fixed monitoring stations.

Figure 15 illustrates the calculated and directly sampled suspended sediment concentrations in g m^{-3} for the ship transect of September 13, 1985 (determined from the visible red MOMS channel) as a function of both time and ship location in an identical manner to the seston concentration curve of Figure 11. The similarities between Figures 15 and 11 are immediately apparent, and the possible impact of ship-induced bottom resuspension is once again a most noticeable feature of Figure 15.

Figure 16 illustrates the remote (and directly sampled) suspended sediment concentrations for the ship transect of September 14, 1985, once again, utilizing the MOMS visible red channel volume reflectance data as the source of remote estimation of suspended sediment concentrations.

Figures 17 and 18 are the visible green channel (0.52 μ - 0.60 μ) equivalents of the red channel curves of Figures 15 and 16. Once again the remotely determined MOMS estimates of suspended sediment concentrations are displayed as the continuous curve while the discontinuous horizontal bars represent the suspended sediment concentrations measured by direct sampling at the fixed monitoring stations.

A very high degree of consistency among the seston and suspended sediment concentrations as determined from the remote measurements of the upwelling radiance by MOMS in the red and the green portions of the visible spectrum, are clearly seen from Figures 11 through 18. Consequently, the discussions applicable to the remote and direct seston concentration determinations (Figures 11 through 14) are equally applicable to the remote and direct suspended sediment concentration determinations (Figures 15 through 18).

It must be emphasized that the predicted concentrations of seston and suspended sediments in this study resulted from correlations between remotely estimated values of $R_{VS}(0)$ and directly measured values of seston and suspended sediment concentrations. No absorption and/or scattering "cross-sections" were calculated for either the seston or suspended sediment particulates, since the direct sampling techniques (both optical and non-optical) were not as rigorously comprehensive as the large scale activities previously conducted in Lake Ontario (Bukata et al., 1979; 1981a; 1981b; 1981c). It is, however, of interest to compare the results of the current predictions

of suspended sediment concentrations over Lake St. Clair (based on correlation techniques) with predictions of suspended sediments (resulting from the use of the optical "cross-sections") determined from the earlier Lake Ontario work. It must be realized, of course, that departures from identical predictive values encountered in such a comparison, are not necessarily due solely to the differences in both the nature and rigor of the techniques employed in the water quality modelling activities, but could very possibly be a consequence of dissimilarities between the nature and optical behaviour of the classes of particulates indigenous to the two distinct aquatic locations.

Figure 19 presents a comparison between the suspended sediment concentration values as a function of $R_{VS}(0)$ for the visible red (0.63 μ - 0.69 μ) MOMS channel as predicted from the current Lake St. Clair study (Curve A) and the former Lake Ontario study (Curve B). Curve B was calculated on the assumption that the Lake Ontario chlorophyll a concentrations were included in the range 0-10 mg m^{-3} and the dissolved organic carbon concentrations were included in the range 1-4 g m^{-3}. No per se Lake St. Clair chlorophyll or dissolved organic carbon concentrations were considered in the calculation of Curve A. While Curves A and B display an obvious similarity in basic shape, they also display an obvious dissimilarity. In addition to Curve B (Lake Ontario) initiating its low sediment concentration onset at a larger $R_{VS}(0)$ red value, the Lake Ontario curve is

characterized by a faster rising slope than is Curve A (Lake St. Clair). The two curves intersect and reverse the sign of the relative difference between their predictions at intermediate to large values of encountered suspended sediment concentrations. Despite the differences in the methodologies utilized in these two optical environmental studies, the differences in the predictive capabilities of these two models is indicative of the difficulties which must be anticipated when environmental models appropriate to one set of environmental parameters are considered for application to another possibly dissimilar set of environmental parameters.

CONCLUDING REMARKS

Methdologies have been developed to enable the calculation of a subsurface spectral volume reflectance from the upwelling spectral radiance and the downwelling spectral solar and sky irradiances. These are optical parameters which are capable of being continuously monitored by MOMS, a dual-chambered, ship-mounted, multispectral reflectance radiometer system. These calculated subsurface volume reflectance values may then be related through water quality modelling techniques to the scattering and absorption centres indigenous to the waters being observed. Thus MOMS provides the capability for continously monitoring water quality indicators in a remote optical manner from an above water-surface vantage position aboard a research vessel.

MOMS data, collected during a September, 1985 study in Lake St. Clair, has been utilized to effect an estimate of seston and suspended sediment concentrations in Lake St. Clair, and logistic difficulties encountered at the fixed in situ sampling stations notwithstanding, MOMS has been demonstrated as being a valuable tool for the continuous monitoring of such turbid water indicators.

Future applications of MOMS to less sediment-laden waters are intended.

REFERENCES

Bukata, R.P., J.H. Jerome, J.E. Bruton, and S.C. Jain. 1979. Determination of Inherent Optical Properties of Lake Ontario Coastal Waters. Appl. Opt. 18, 3926-3932.

Bukata, R.P., J.H. Jerome, J.E. Bruton, S.C. Jain and H.H. Zwick. 1981a. Optical Water Quality Model of Lake Ontario. 1. Determination of the Optical Cross Sections of Organic and Inorganic Particulates in Lake Ontario. Appl. Opt. 20, 1696-1703.

Bukata, R.P., J.H. Jerome, J.E. Bruton, S.C. Jain and H.H. Zwick. 1981b. Optical Water Quality Model of Lake Ontario. 2. Determination of Chlorophyll a and Suspended Mineral Concentrations of Natural Waters from Submersible and Low Altitute Optical Sensors. Appl. Opt. 20, 1704-1714.

Bukata, R.P., J.H. Jerome, and J.E. Bruton. 1981c. Validation of a Five-Component Optical Model for Estimating Chlorophyll a and Suspended Mineral Concentrations in Lake Ontario. Appl. Opt. 20, 3472-3474.

Bukata, R.P, J.E. Bruton, and J.H. Jerome. 1985. Application of Direct Measurements of Optical Parameters to the Estimation of Lake Water Quality Indicators. Env. Can. IWD Scientific Series No. 140, 35 pp.

Cox, C. and W. Munk. 1955. Some Problems in Optical Oceanography. J. Mar. Res. 14, 63-78.

Duntley, S.Q., R.W. Austin, W.H. Wilson, C.F. Edgerton, and S.E. Moran. 1974. Ocean Color Analysis. Scripps Institution of Oceanography, San Diego. SIO Ref. 74-10, 67 pp.

Gordon, J.I. 1969. Directional Radiance (Luminance) of the Sea Surface. Scripps Institution of Oceanography, San Diego. SIO Ref 69-20.

Jerlov, N.G. 1984. Marine Optics, Elsevier, New York, 231 pp.

Maul, G.A. 1985. Introduction to Satellite Oceanography, Martinus Nijhoff Publishers, Dordrecht/Boston/Lancaster, 606 pp.

Payne, R.E. 1972. Albedo of the Sea Surface. J. Atmos. Sci. 29, 959-970.

Watson, A.S., F.E. Roy, and J. Dolanjski. 1982. Handbook Notes for Shipboard Reflectance Radiometer System. Unpublished Manuscript, Engineering Services Section, National Water Research Institute, 44 pp.

Table I. Results of exponential correlations between the calculated
normalized spectral values of volume reflectance* observed
by MOMS and sampled concentrations of seston S and suspended
sediments SS.

Wavelength	Regressions	Correlation Coefficient r	Standard Deviation of the Errors σ
Green (0.52 µ–0.60 µ)	$S = 1.43\ e^{10.5\ R_{VG}}$	0.86	±22%
	$SS = 1.06\ e^{11.0\ R_{VG}}$	0.87	±22%
Red (0.63 µ–0.69 µ)	$S = 2.22\ e^{25.8\ R_{VR}}$	0.85	±24%
	$SS = 1.69\ e^{26.9\ R_{VR}}$	0.86	±24%
Infra-red (0.80 µ–1.1 µ)	$S = 2.62\ e^{73.3\ R_{VIR}}$	0.65	±36%
	$SS = 2.06\ e^{74.1\ R_{VIR}}$	0.64	±38%

*The spectral volume reflectances R_{VG}, R_{VR} and R_{VIR} are the
green, red and infra-red values, respectively, of the $R_{VS}(0)$ term in
equations (22) and (23).

FIGURE CAPTIONS

Figure 1: Schematic representation of the dual radiometer system, MOMS.

Figure 2: Estimated values of Q as a function of solar zenith angle for large backscattering probability (Curve A), low backscattering probability (Curve B), and arithmetic mean (Curve C).

Figure 3: Curve illustrating the impact on $R_{VS}(\theta)$ of varying θ.

Figure 4: Schematic map of Lake St. Clair illustrating ship transects and sampling stations.

Figure 5: Exponential regression between the green volume reflectance and the total seston concentration.

Figure 6: Esponential regression between the green volume reflectance and the suspended sediment concentration.

Figure 7: Exponential regression between the red volume reflectance and the total seston concentration.

Figure 8: Exponential regression between the red volume reflectance and the suspended sediment concentration.

Figure 9: Exponential regression between the infra-red volume reflectance and the total seston concentration.

Figure 10: Exponential regression between the infra-red volume reflectance and the suspended sediment concentration.

Figure 11: Total seston concentrations as determined from the visible red channel of MOMS on September 13, 1985 (continuous curve) along with the seston concentrations determined from direct sample collection (non-continuous lines).

Figure 12: Total seston concentrations as determined from the visible red channel of MOMS on September 14, 1985 (continuous curve) along with the seston concentrations determined from direct sample collection (non-continuous lines).

Figure 13: Total seston concentrations as determined from the visible green channel of MOMS on September 13, 1985 (continuous curve) along with the seston concentrations determined from direct sample collection (non-continuous lines).

Figure 14: Total seston concentrations as determined from the visible green channel of MOMS on September 14, 1985 (continuous curve) along with the seston concentrations determined from direct sample collection (non-continuous lines).

Figure 15: Suspended sediment concentrations as determined from the visible red channel of MOMS on September 13, 1985 (continuous curve) along with the suspended sediment concentrations determined from direct sample collection (non-continuous lines).

Figure 16: Suspended sediment concentrations as determined from the visible red channel of MOMS on September 14, 1985 (continuous curve) along with the suspended sediment concentrations determined from direct sample collection (non-continuous lines).

Figure 17: Suspended sediment concentrations as determined from the visible green channel of MOMS on September 13, 1985 (continuous curve) along with the suspended sediment concentrations determined from direct sample collection (non-continuous lines).

Figure 18: Suspended sediment concentrations as determined from the visible green channel of MOMS on September 14, 1985 (continuous curve) along with the suspended sediment concentrations determined from direct sample collection (non-continuous lines).

Figure 19: Suspended sediment concentrations as a function of visible red volume reflectance as predicted from correlations performed in the current Lake St. Clair study (Curve A) and as predicted from "cross sections" determined in Lake Ontario (Curve B).

ROTATING SOLAR OCCLUDER

UPWARD-VIEWING 4-CHANNEL RADIOMETER ASSEMBLY

HEMISPHERICAL PLEXIGLASS WINDOW

SHIP BOOM

DOWNWARD-VIEWING 4-CHANNEL RADIOMETER ASSEMBLY

AIR

WATER

FIG. 1

FIG. 2

$$R_{VS}(\theta) = \frac{R_{VS}(0)}{\cos(\theta_r)}$$
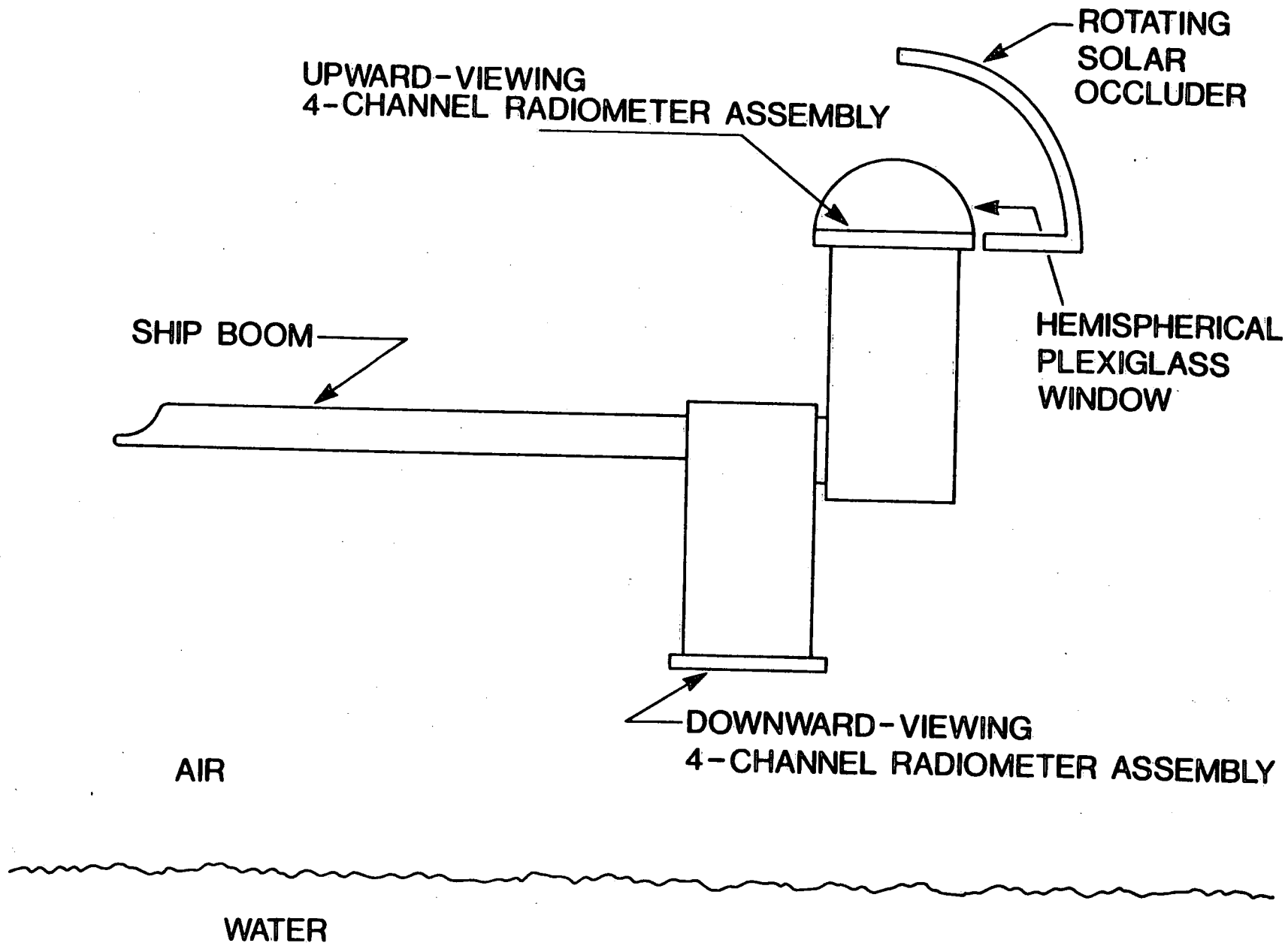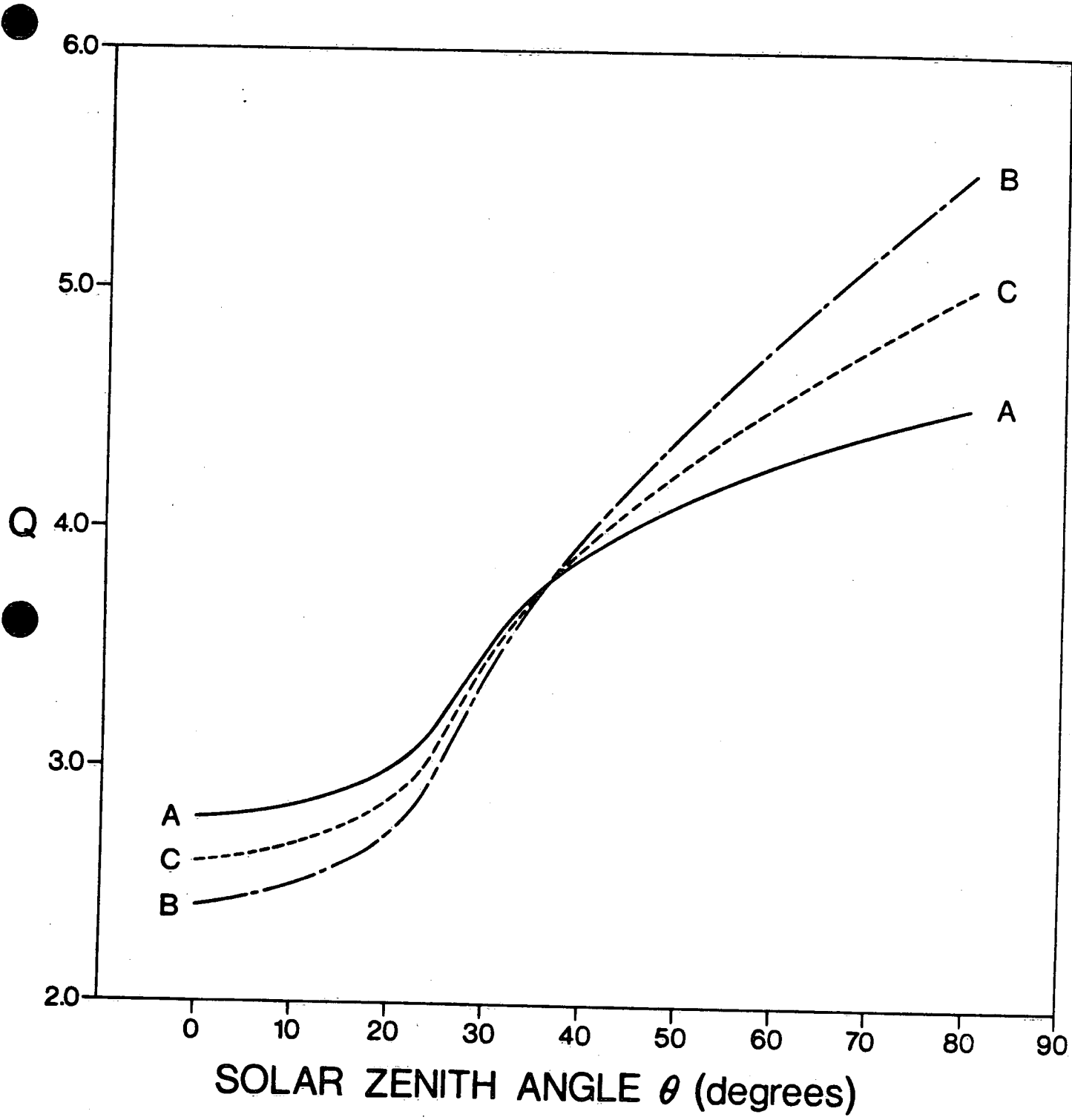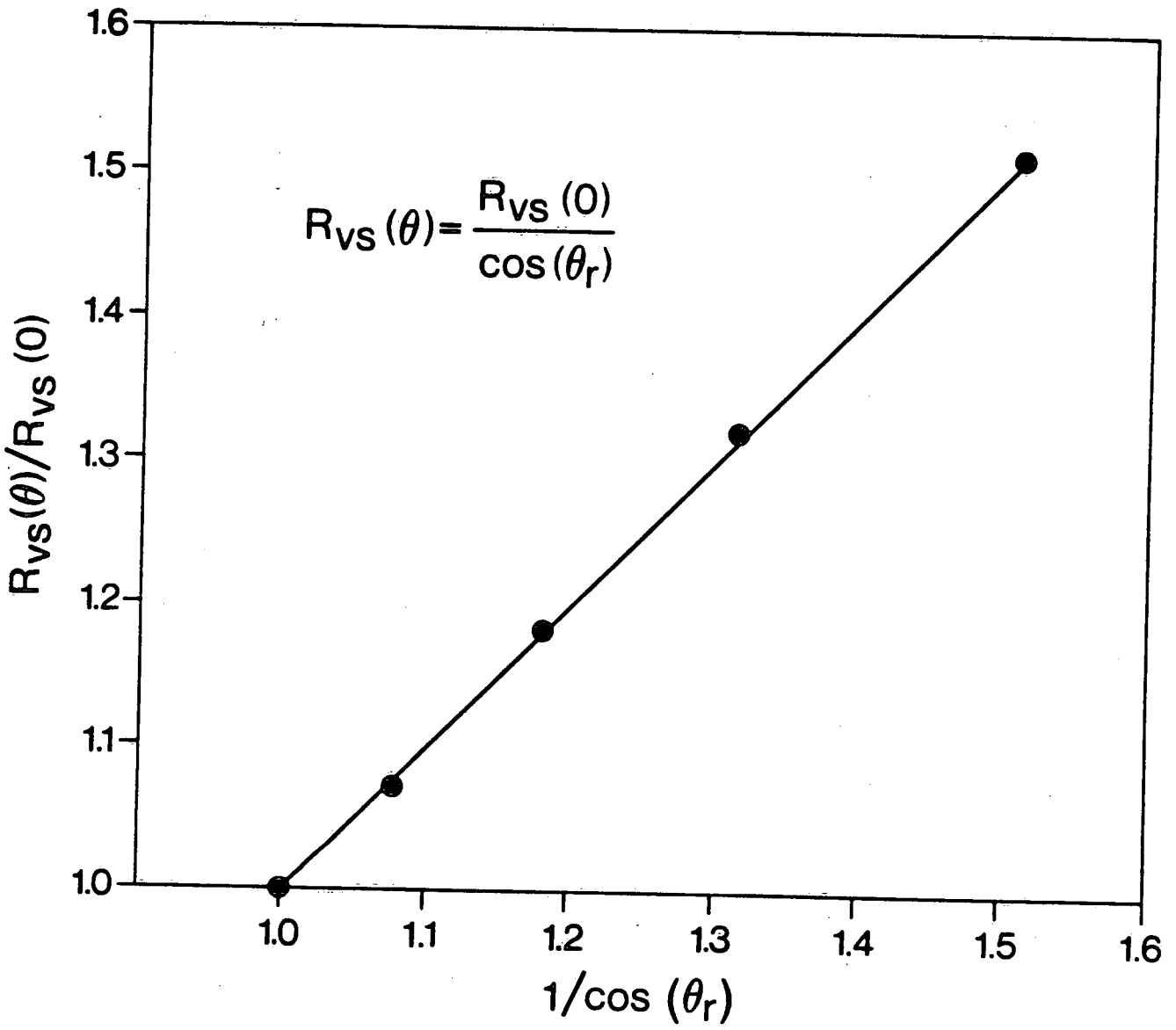
FIG. 3

SEPT 13 ———·—·—·———
SEPT 14 ————————
SEPT 16 ——— —— ———
SEPT 19 ·······················

82°30'W

42°40'N

61
62
63
64
19
65
66
67
1
68
69
60
70
19
71
20
72
73
74
75
76
77
78
79
80
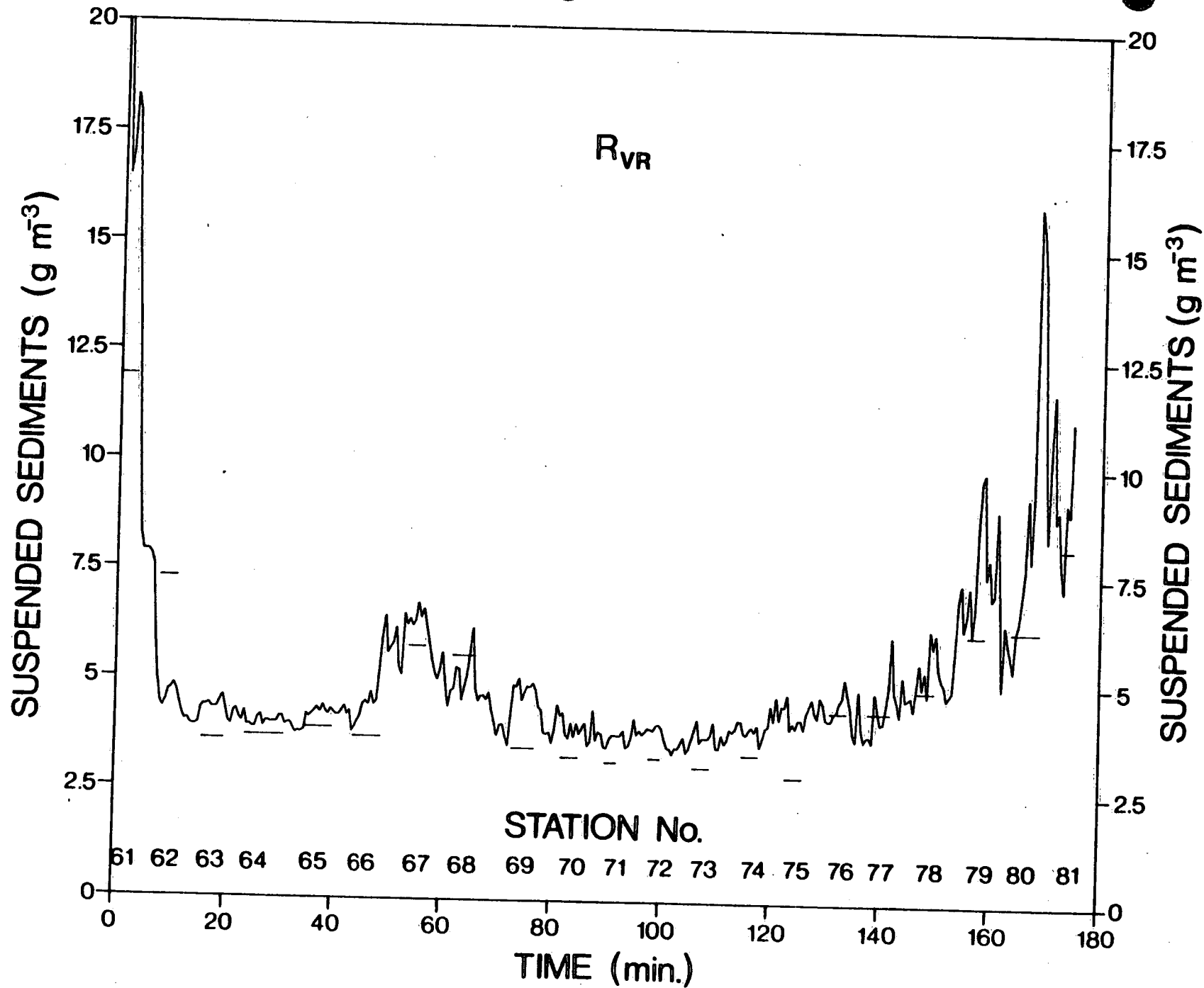81

LAKE ST. CLAIR

83°00'W

42°15'N

FIG. 4

FIG.5

FIG.6

RED VOLUME REFLECTANCE
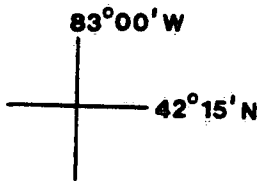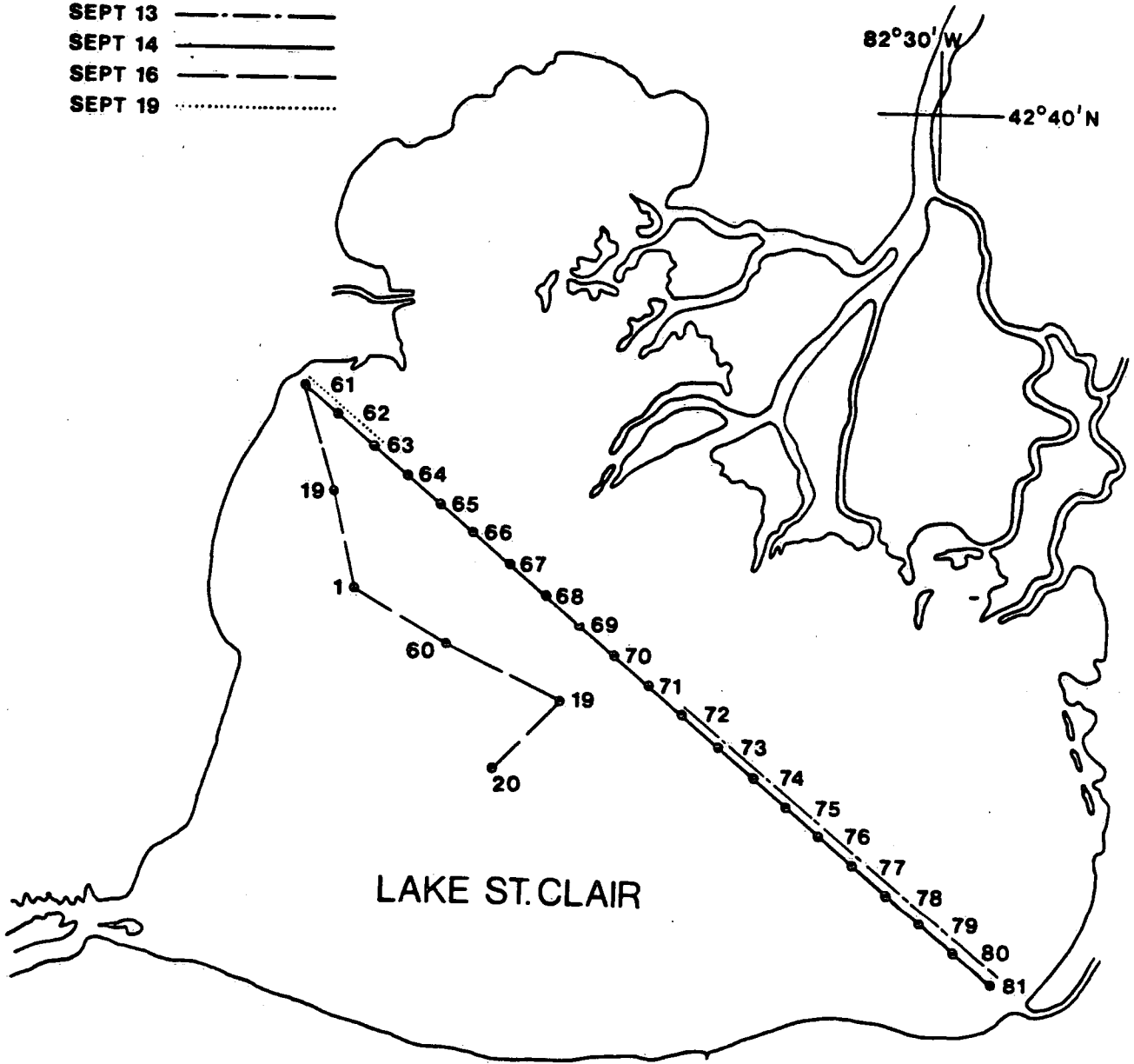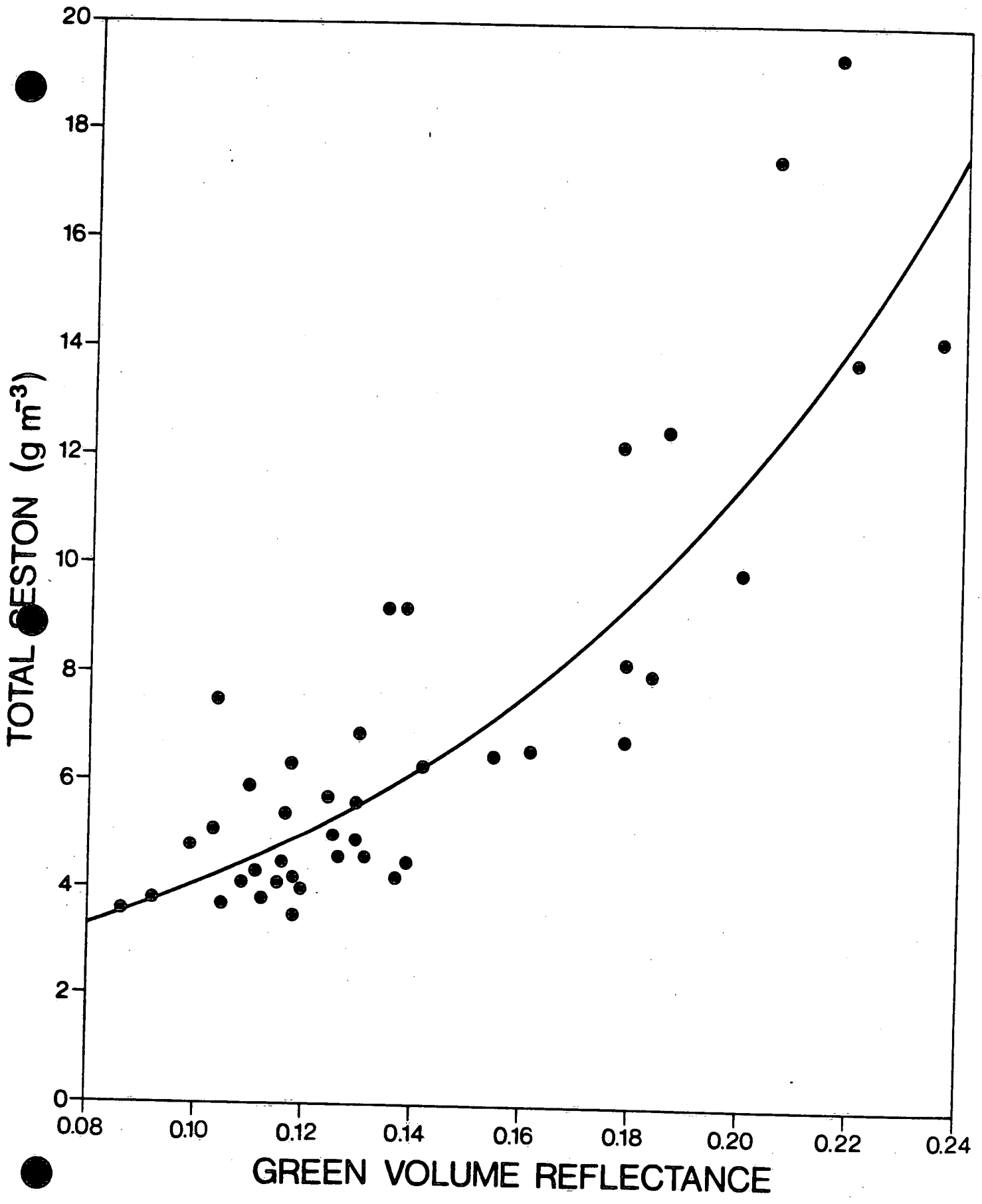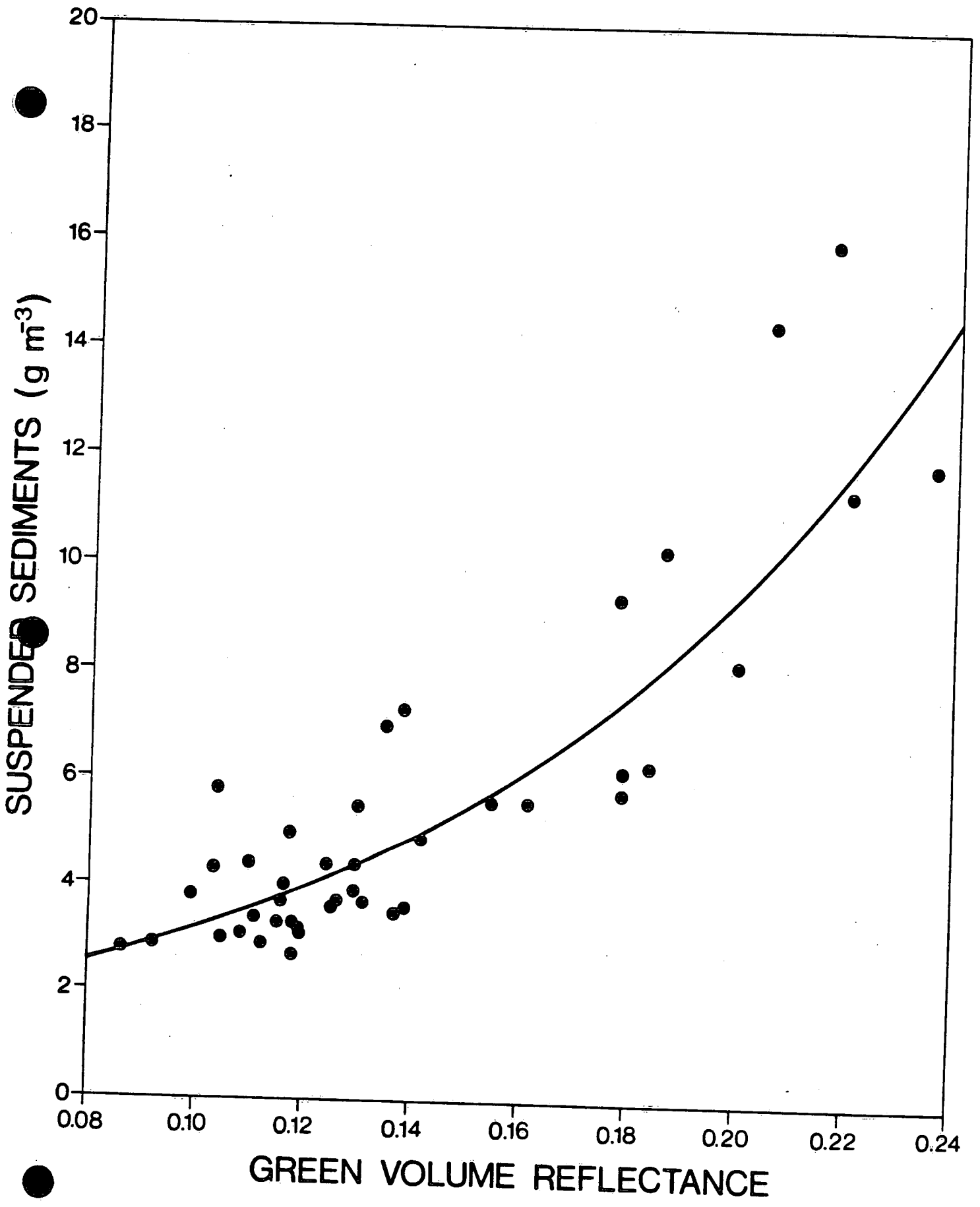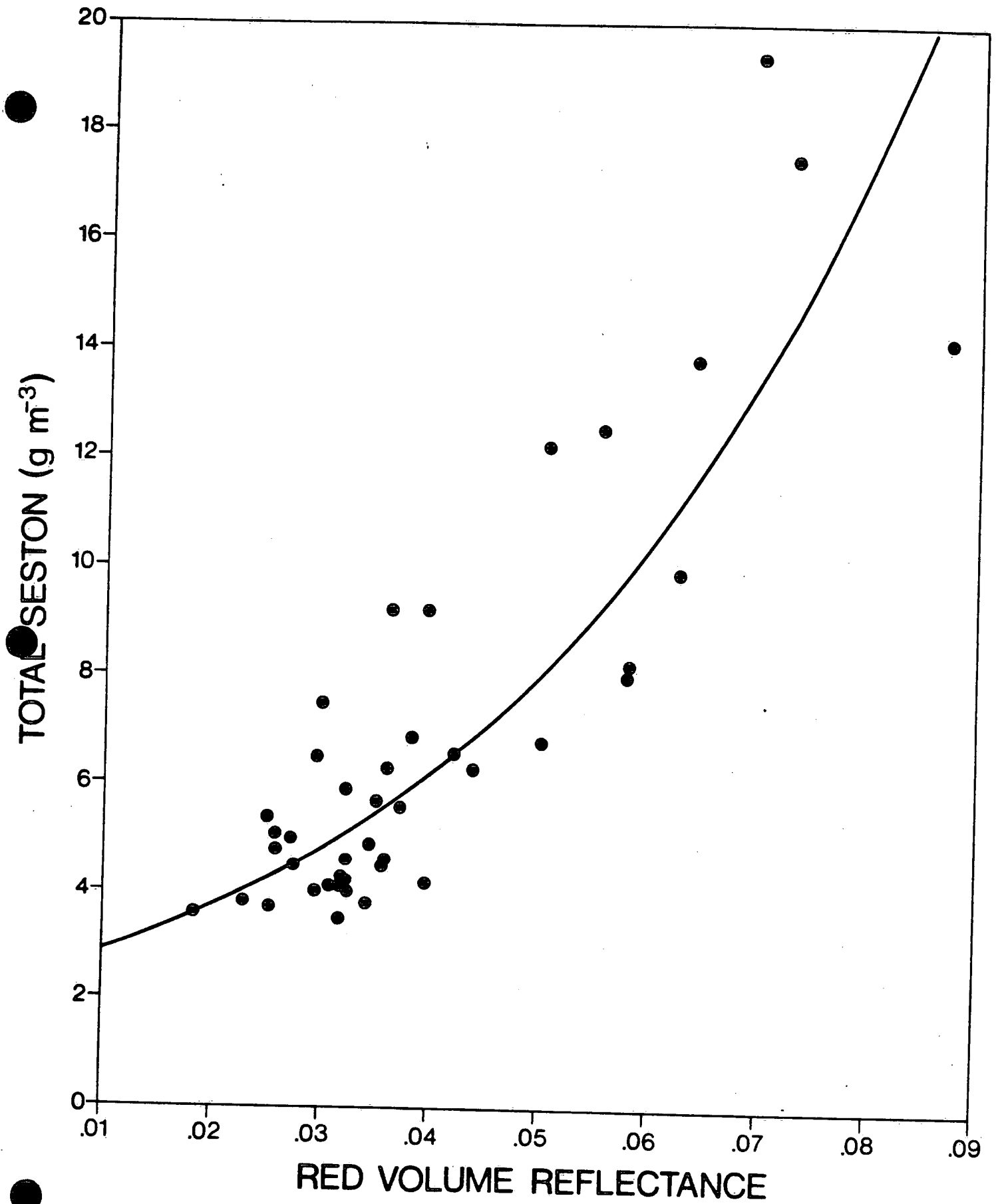
FIG.7
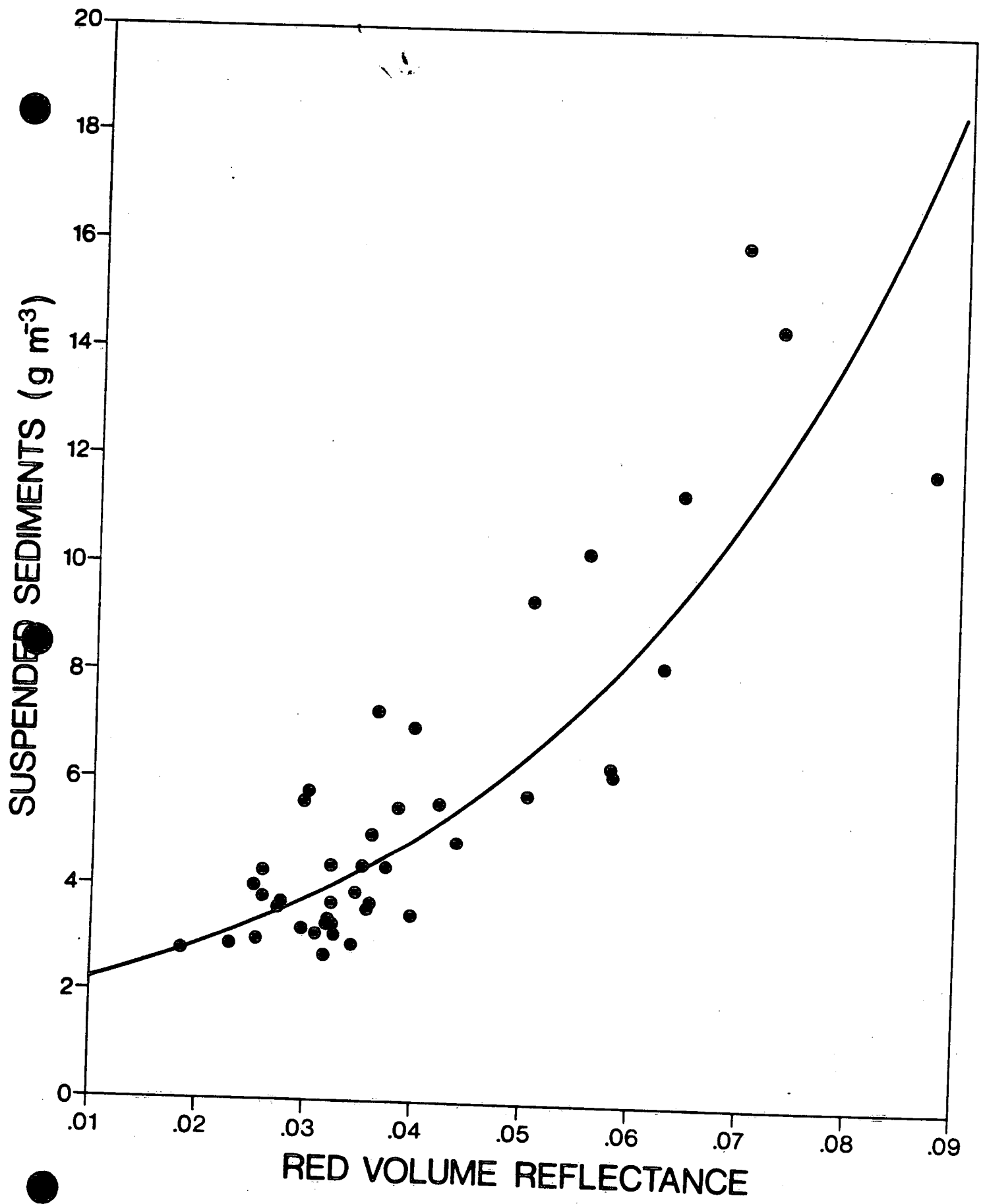
FIG. 8
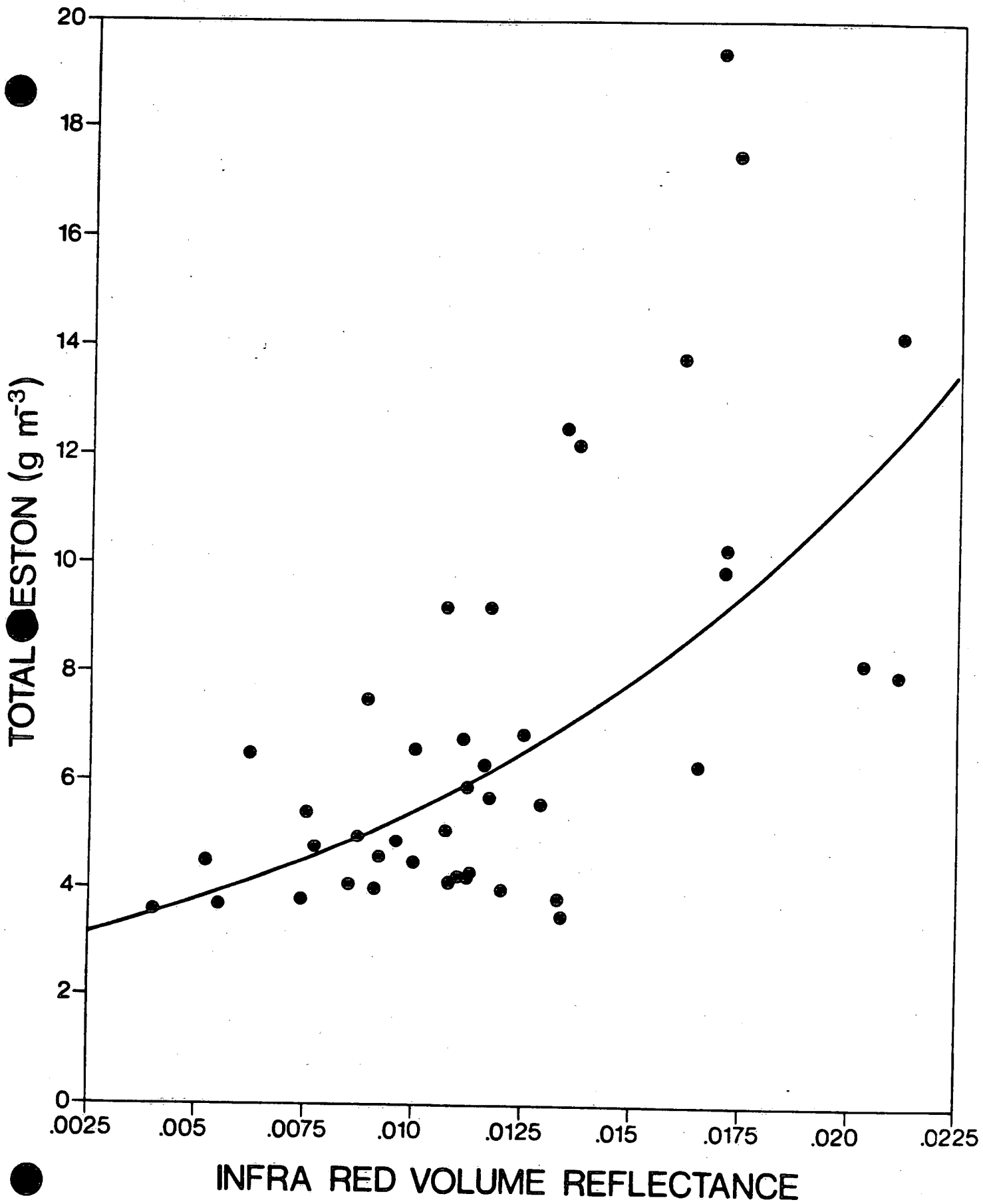
FIG. 9
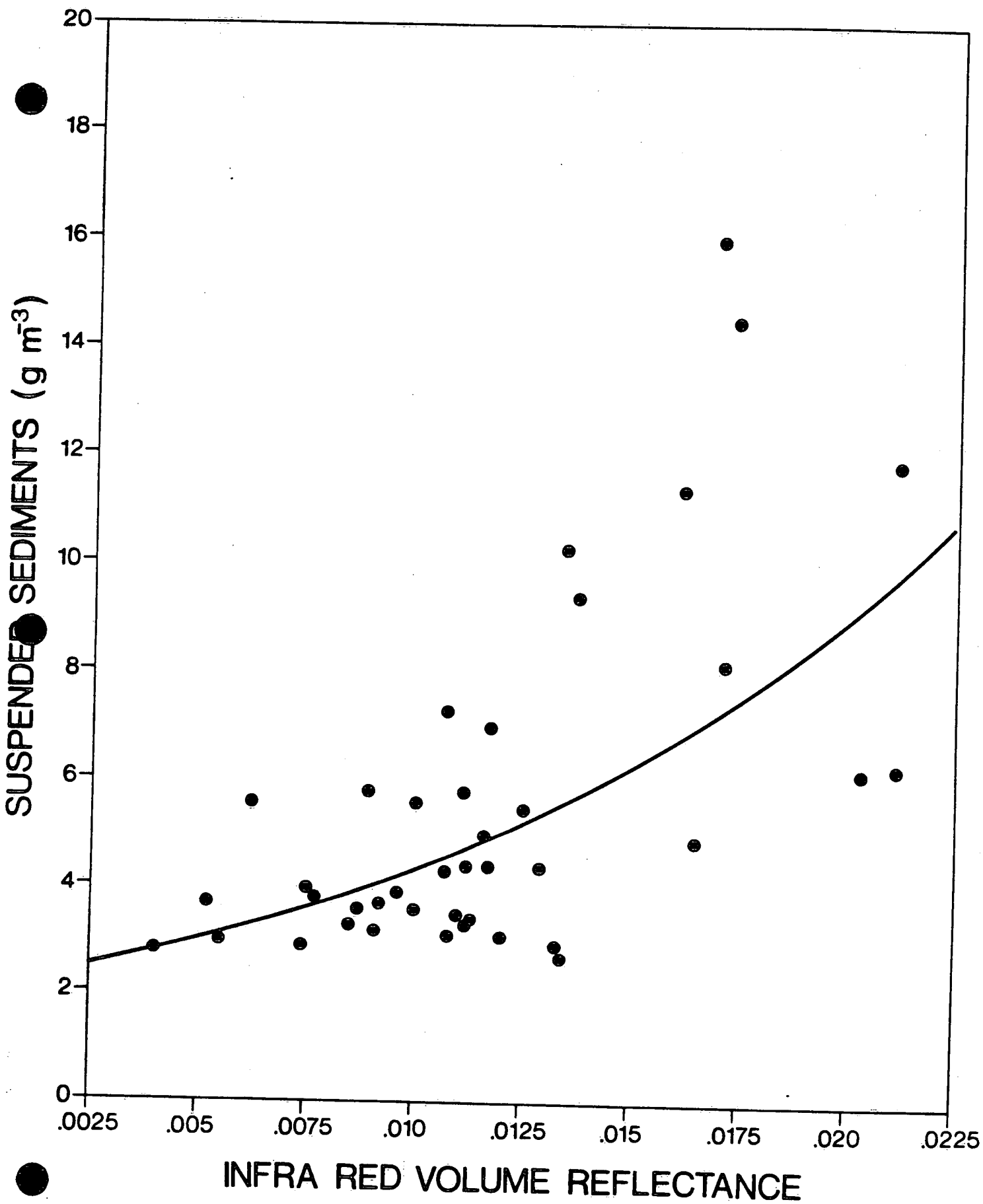
FIG. 10

FIG. 11

FIG. 12

FIG. 13

FIG. 14

R_{VG}

TOTAL SESTON (g m^{-3})

STATION No.

61 62 63 64 65 66 67 68 69 70 71 72 73 74 75 76 77 78 79 80 81

TIME (min.)
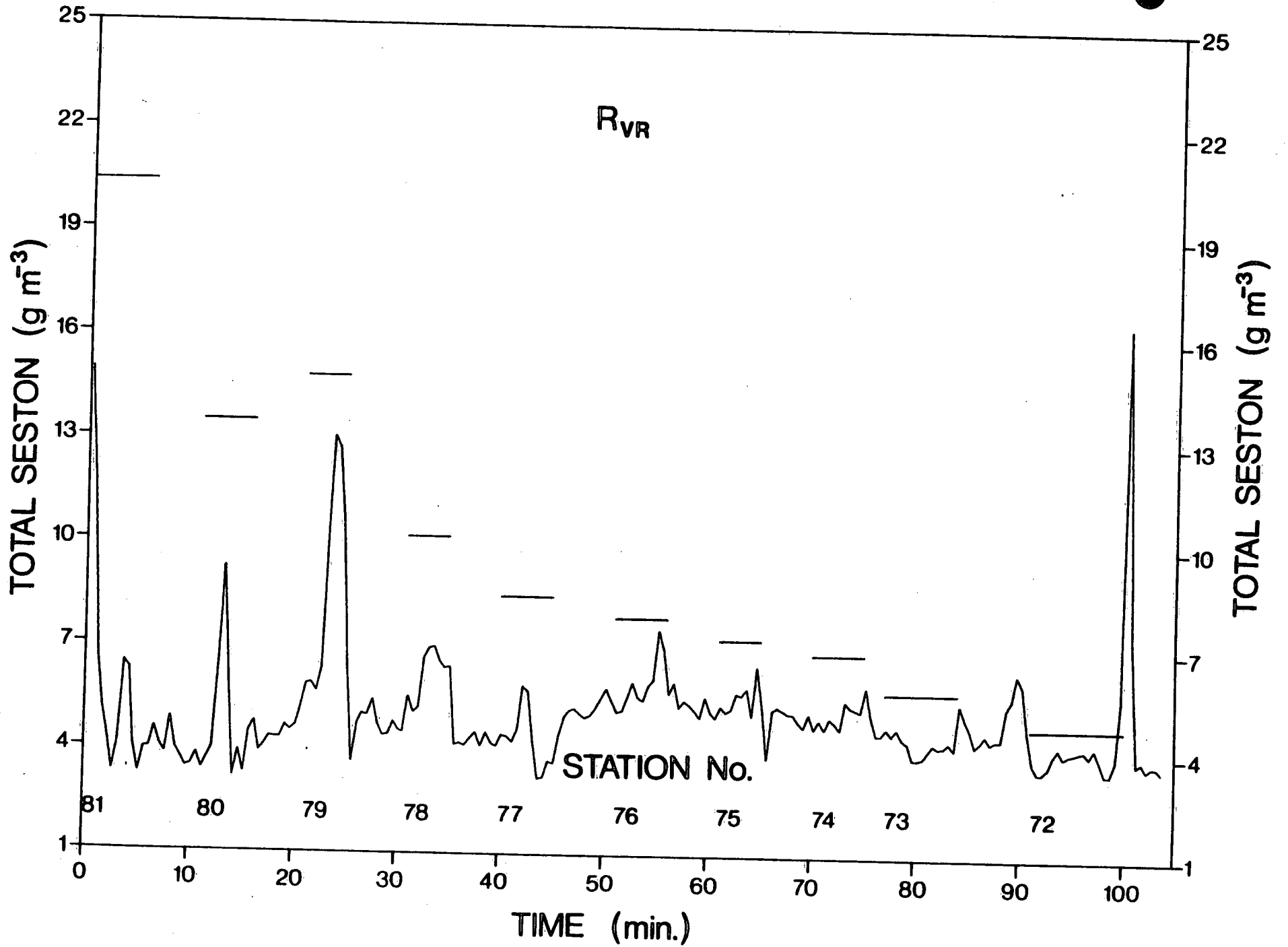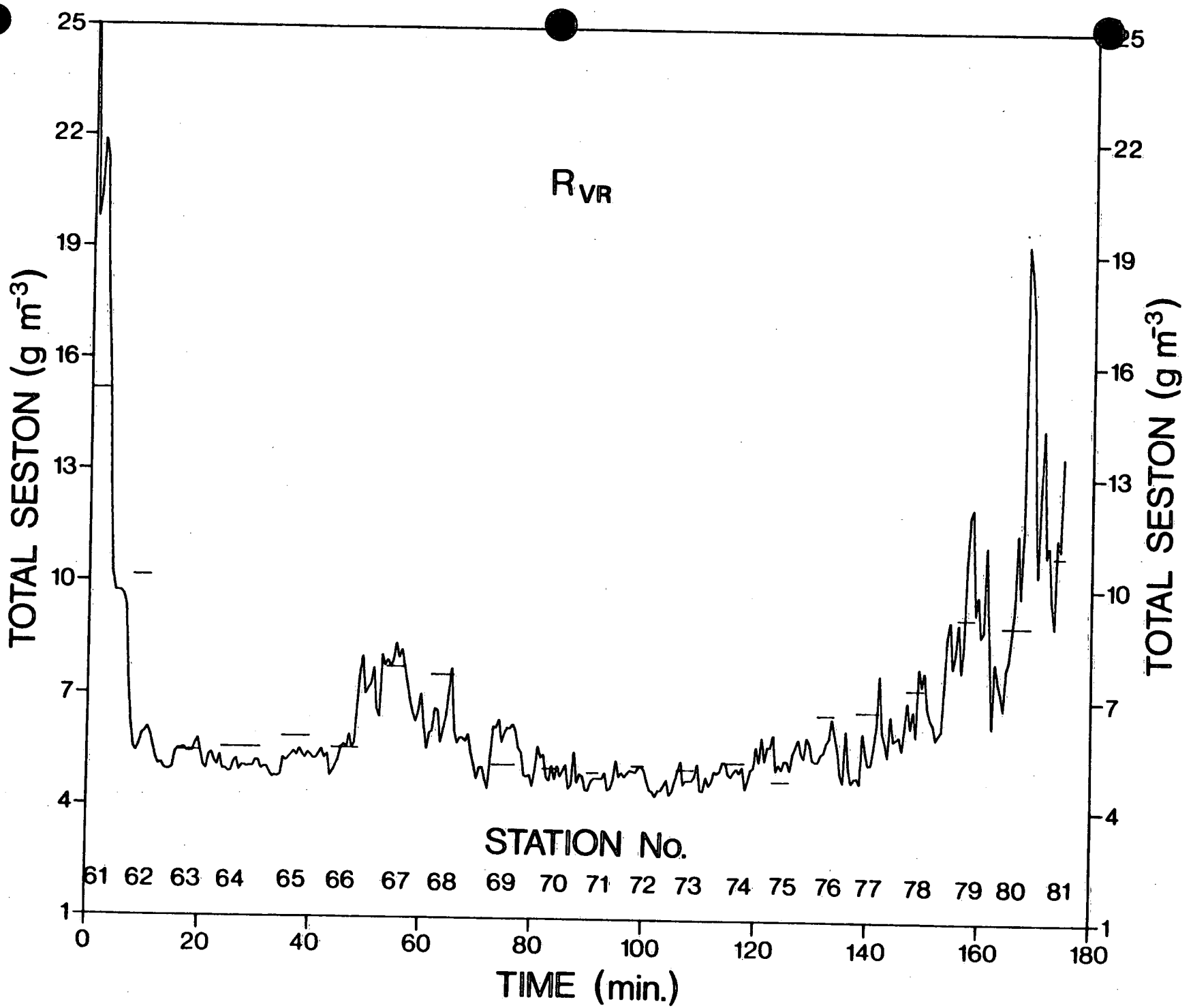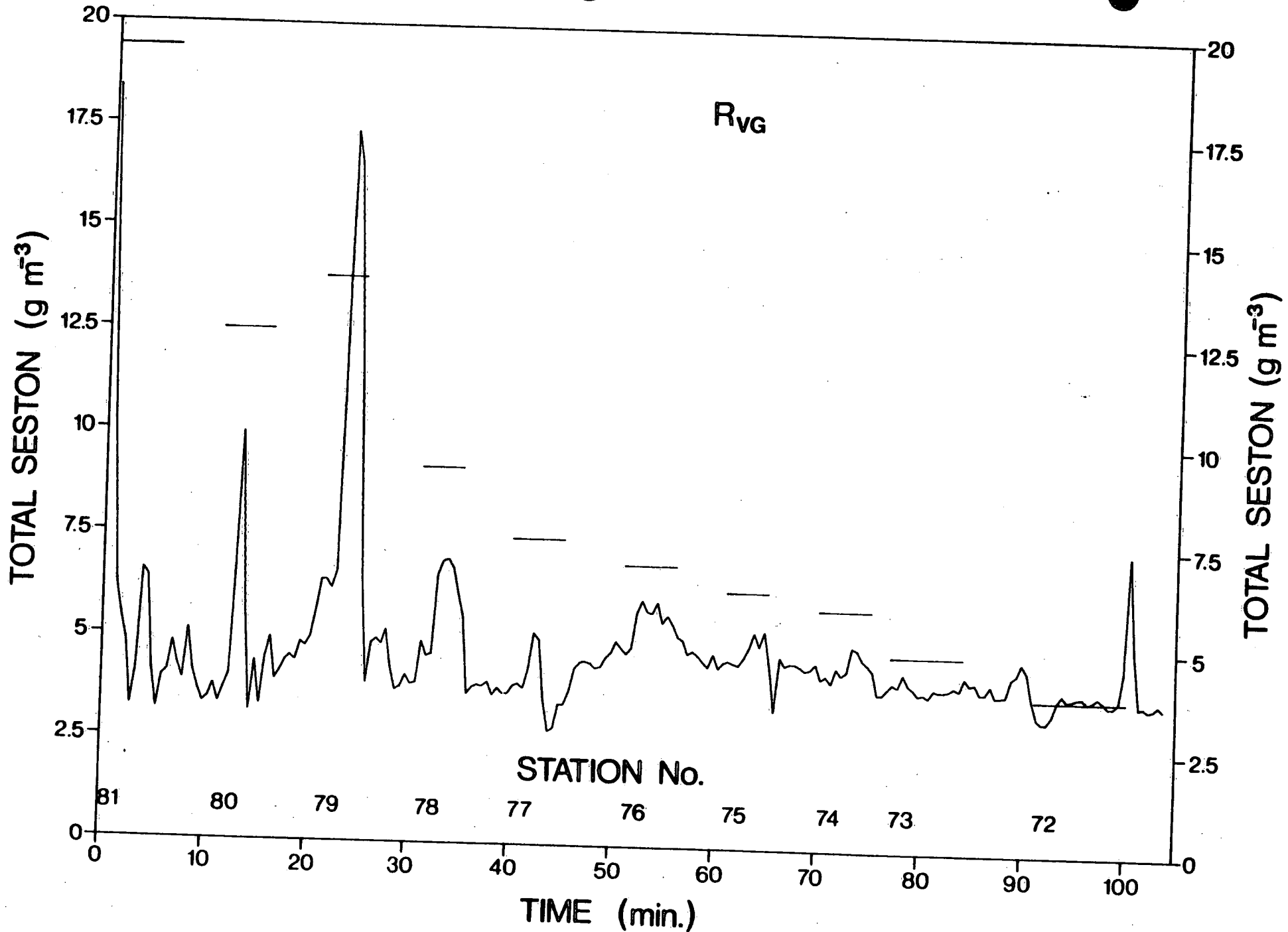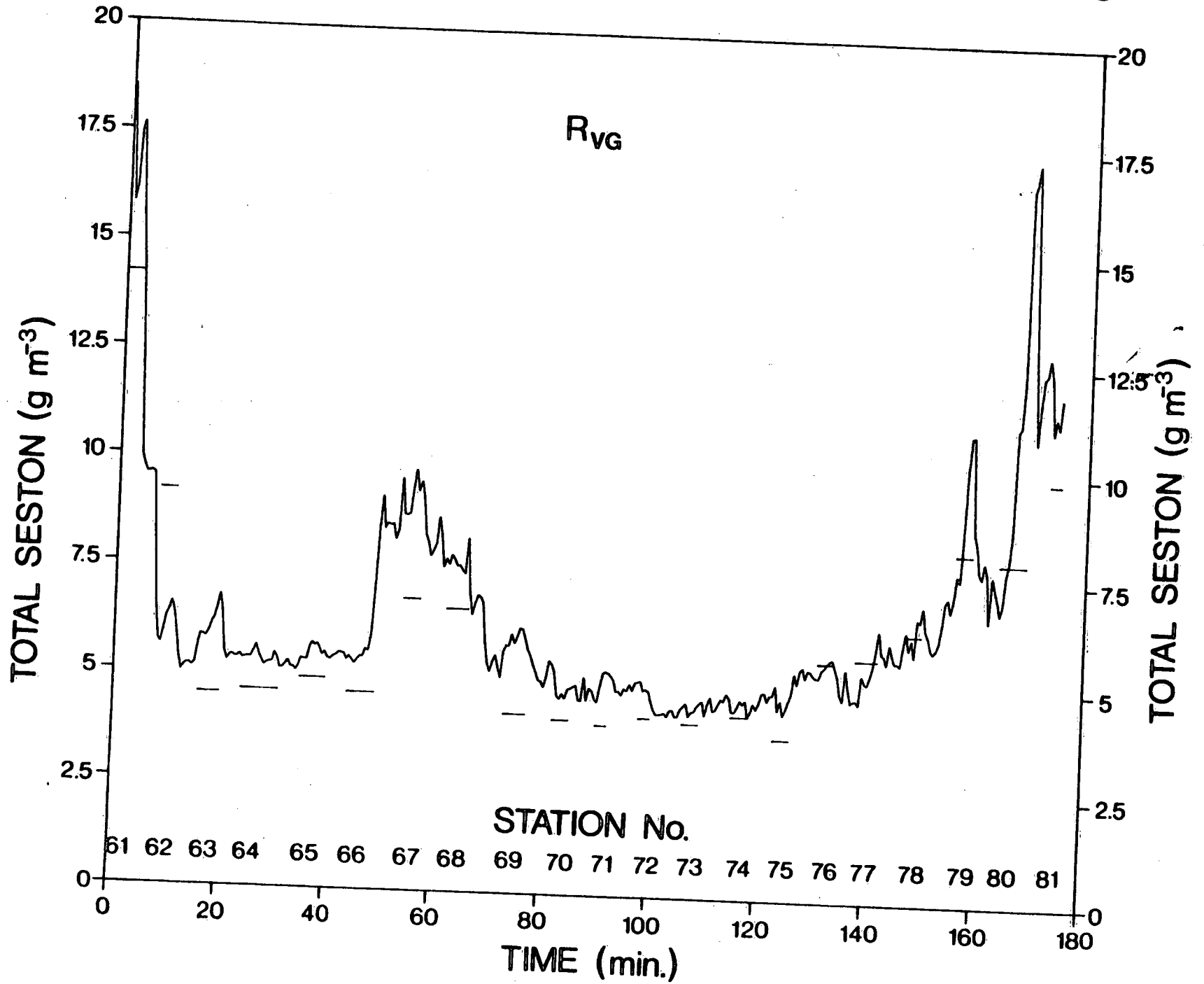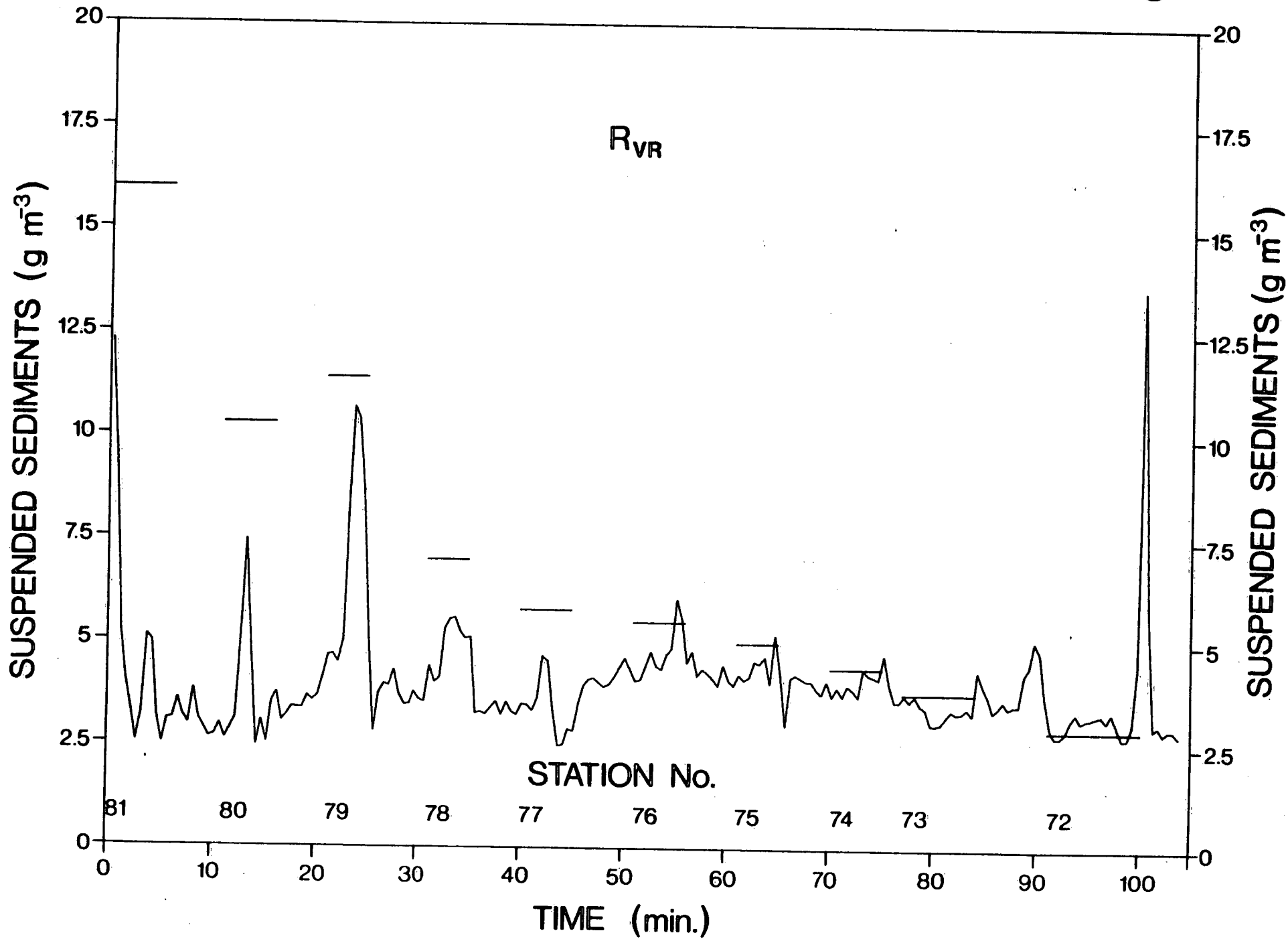
FIG. 15

FIG. 16

FIG. 17

FIG. 18

FIG. 19